Delamination of a thin sheet from a soft adhesive Winkler substrate

Oz Oshri,[1,*] Ya Liu,[1] Joanna Aizenberg,[2,3,4] and Anna C. Balazs[1]

[1]*Chemical Engineering Department, University of Pittsburgh, Pittsburgh, Pennsylvania 15261, USA*

[2]*John A. Paulson School of Engineering and Applied Sciences, Harvard University, Cambridge, Massachusetts 02138, USA*

[3]*Wyss Institute for Biologically Inspired Engineering and Kavli Institute for Bionano Science and Technology, Harvard University, Cambridge, Massachusetts 02138, USA*

[4]*Department of Chemistry and Chemical Biology, Harvard University, Cambridge, Massachusetts 02138, USA*

(Received 19 March 2018; published 20 June 2018)

A uniaxially compressed thin elastic sheet that is resting on a soft adhesive substrate can form a blister, which is a small delaminated region, if the adhesion energy is sufficiently weak. To analyze the equilibrium behavior of this system, we model the substrate as a Winkler or fluid foundation. We develop a complete set of equations for the profile of the sheet at different applied pressures. We show that at the edge of delamination, the height of the sheet is equal to $\sqrt{2}\ell_c$, where ℓ_c is the capillary length. We then derive an approximate solution to these equations and utilize them for two applications. First, we determine the phase diagram of the system by analyzing possible transitions from the flat and wrinkled to delaminated states of the sheet. Second, we show that our solution for a blister on a soft foundation converges to the known solution for a blister on a rigid substrate that assumed a discontinuous bending moment at the blister edges. This continuous convergence into a discontinuous state marks the formation of a boundary layer around the point of delamination. The width of this layer relative to the extent length of the blister, ℓ, scales as $w/\ell \sim (\ell_c/\ell_{ec})^{1/2}$, where ℓ_{ec} is the elastocapillary length scale. Notably, our findings can provide guidelines for utilizing compression to remove thin biofilms from surfaces and thereby prevent the fouling of the system.

DOI: 10.1103/PhysRevE.97.062803

I. INTRODUCTION

In the past few decades, there has been renewed interest in the behavior of thin elastic sheets due to the findings that these films form novel patterns under confinement [1–4]. In particular, thin elastic sheets that are adhered to soft foundations present rich morphological structures, such as smooth wrinkles and localized folds [5–9], or stress focusing patterns, such as crumpled structures and creases [10,11]. Although these structures depend strongly on the system set-up, i.e., the geometry and the external forces, they all originate from the same competition between the energetics of the substrate and the elastic sheet.

The nature of the pattern formation changes dramatically when the latter two energies become comparable to the adhesion energy, which characterizes the strength of bonding between the elastic sheet and the substrate. Under these conditions, it is often experimentally observed that the sheet delaminates from the substrate [12,13]. This detachment mechanism gives rise to wealth of new structures. For example, a thin sheet peeled from an adhesive substrate revealed fingering instabilities [14] and triangular shapes [15–17]. The delamination of a flat sheet placed in contact with an adhesive, spherical substrate displayed branched, wavy patterns [18] or axisymmetric wrinkles [19].

Spatially localized delaminated regions within these patterns are generally referred to as blisters. Blisters are of special importance in the study of fracture mechanics [20,21] and in the measurements of the adhesion energy [22] because their formation is tractable both experimentally and theoretically. The formation of a two dimensional blister in the form of a telephone cord was analyzed in Refs. [23,24]. Another example is given in Ref. [25] where a circular thin sheet was placed on a fluid substrate and displaced upwards from its center by an indentor. When a blister formed, its border presented five different morphologies, from a smooth circular shape to a sharp triangular boundary.

In this paper, we focus on a particular system set-up of a one-dimensional blister and consider a thin sheet that is adhered to a Winkler foundation or a fluid substrate and is then uniaxially compressed. The restoring force that is provided by the Winkler model is relatively simple; it is represented by harmonic springs that only deform in the vertical direction. Under some restrictions [26], the Winkler model mimics the behavior of a soft elastic substrate [27]. Although this system has been analyzed extensively when the sheet is completely adhered to the substrate (presenting wrinkles and fold states) [7,9,28–30], less attention was given to the possible transition from an adhered state to a delaminated pattern. One study that approached this problem was presented in Ref. [27], where the researchers considered the delamination of a heavy sheet from a fluid substrate. In the latter study, a sheet with nonnegligible weight was placed on a fluid substrate and uniaxially compressed. At a critical confinement, a transition to a delaminated state occurred. This state was governed by two regimes: One is a central blister that mimics the shape of a heavy elastica [31–33], and the second is an adhered regime

*ozo2@pitt.edu

that consists of a sinusoidal decaying pattern, which mimics the shape of a floating elastica [7].

The analysis presented here differs from the above study [27] in two aspects. First, we neglect gravitational effects. While in Ref. [27] the gravitational energy of the sheet was considered as the dominant mechanism for the formation of a blister, here we neglect this contribution and show that, in general, a blister can form independent of the weight of the sheet. Consequently, we shed light on the regime where the elastocapillary length-scale is dominant instead of the elastogravitational length-scale. Second, we relax the inextensibility assumption that was placed in Ref. [27]. This allows us to analyze the flat-to-blister transition, in addition to the wrinkles-to-blister transition that was analyzed in Ref. [27].

An important outcome of the present model is the convergence of its solution to that of a large blister on a rigid substrate [34]. Notably, our model assumes a continuous transition between the two regions of the sheet, the delaminated and adhered parts. However, the prior model on a rigid substrate [34], assumes discontinuous bending moments at the blister edges. Although the latter condition has been extensively justified either analytically by an energy minimization method [35–37] and the J-integral procedure [20,38] or experimentally [34,39], it nevertheless prescribes a nonintuitive discontinuity in the profile of the sheet. The convergence of the two models, for soft and rigid substrates, has two signicant implications. First, it justifies the moment-discontinuity from a new perspective; namely, it shows a continuous convergence into the discontinuity. Second, when a discontinuity in the bending moment is prescribed, it obviously masks very sharp gradients that occur over very small distances, i.e., a boundary layer. The present solution provides the details of this layer and allows us to extract its characteristics, such as the stress profiles around the point of delamination and the penetration length inside the substrate. To the best of our knowledge, this is the first time that this condition is obtained as an asymptotic limit of a continuous shape.

We note that these studies are relevant to investigations of the delamination of biofilms from soft or fluidlike substrates. Biofilms are formed from a combination of cells and the extracellular matrix of the individual cells [40,41]. The adhesion of a biofilm to the underlying substrate plays a crucial role in the fouling of submerged surfaces and consequently, the deterioration of devices encompassing such surfaces. In the continuum limit, this biofilm can be viewed as a viscoelastic thin layer, or to leading order, as a thin elastic sheet. Indeed, the detachment patterns of biofilms mimic the ones that are observed on thin sheets [40,42]. Hence, these studies can help pinpoint regions in parameter space where an applied compressive force can be utilized to prevent the biofouling of the substrate.

The paper is organized as follows. In Sec. II, we write the energy functional of the system and minimize it to obtain a complete set of equations for the configuration of the sheet. Under some assumptions, we solve this set of equations in Sec. III and then utilize the solutions for two applications. First, in Sec. IV, we obtain the critical displacement at which a flat or a wrinkled sheet is transformed into a small blister, and second, in Sec. V, we analyze the formation of a boundary layer at the edge of a large blister. Finally, in Sec. VI, we summarize our findings, discuss the relevance of this work to some known experimental results and suggest future extensions.

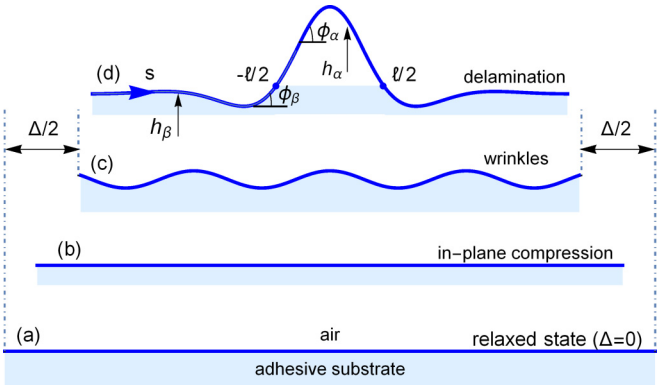

FIG. 1. Schematic evolution of the sheet into a delaminated state. A flat and relaxed sheet (a) that is adhered to a soft substrate and uniaxially compressed can evolve into the delaminated state (d) through one of the following scenarios. First is the flat-to-blister transition, (a)→(b)→(d). The sheet remains flat upon small confinements, $0 < \Delta < \Delta_{\rm fb}$, and then jumps to the delaminated state when $\Delta > \Delta_{\rm fb}$. Second is the wrinkles-to-blister transition, (a)→(b)→(c)→(d). The sheet remains flat up to $\Delta < \Delta_{\rm w} = 2\xi L$. From there on, regular undulations (wrinkles) emerge and remain stable between $\Delta_{\rm w} < \Delta < \Delta_{\rm wb}$. When $\Delta > \Delta_{\rm wb}$ the latter morphology becomes unstable against delamination. The first scenario is dominant if $\Delta_{\rm fb} < \Delta_{\rm w}$; otherwise, and assuming that the adhesion energy, $w_{\rm ad}$, is sufficiently small, the second scenario takes place.

II. FORMULATION OF THE PROBLEM

We consider an extensible flat sheet of relaxed length L, thickness t, and the respective bending and stretching moduli, B and Y. The sheet is adhered to a substrate that has a stiffness K. The sheet is uniaxially confined from the boundaries by either a displacement, Δ, or a pressure, P, such that the external work of shortening the end-to-end length of the sheet is given by $P\Delta$. The deformed configuration is characterized by three fields. One is the angle $\phi(s)$ between the tangent to the sheet and the horizontal axis (see Fig. 1). Second is the compression field $\gamma(s) = d\hat{s}/ds$ where s and $\hat{s}$ are the arc length parameters of the relaxed and compressed configurations, respectively, and third is the height function $h(s)$. These fields are not independent as they are related by the geometrical constraint,

$$\gamma \sin\phi = \frac{dh}{ds}. \tag{1}$$

The deformed profile of the sheet on the xy plane is given parametrically by the position vector $\mathbf{r}(s) = (x(s), h(s))$, where

$$x(s) = \int_{-L/2}^{s} \gamma(s')\cos\phi(s')ds', \tag{2a}$$

$$h(s) = \int_{-L/2}^{s} \gamma(s')\sin\phi(s')ds'. \tag{2b}$$

The total energy of the system, E, is divided into two regimes: (i) the free, delaminated region, $E_{\rm del}$, which is located symmetrically around the sheet center ($s < |\ell/2|$), and (ii) the

adhered region, $E_{\rm adh}$, at the sheet tails ($s > |\ell/2|$),

$$E[\phi(s),\gamma(s),h(s)] = E_{\rm del}[\phi_\alpha(s),\gamma_\alpha(s),h_\alpha(s)] + E_{\rm adh}[\phi_\beta(s),\gamma_\beta(s),h_\beta(s)]. \quad (3)$$

Following the formulation in Ref. [37], we differentiate between the fields in the two regions by the subscripts α and β, where α characterizes the delaminated regime and β characterizes the adhered regime. In addition, since we anticipate the final configuration to be symmetric with respect to the y axis, we consider only the half-sheet, $s \in [0, L/2]$ and multiply the energy by a factor of two. Note that the delamination length, ℓ, is *a priori* unknown. It will be determined to minimize the total energy of the system.

In the delaminated region, the sheet is free and therefore there is an energetic penalty that is associated with the bending and stretching of this delaminated region. This energetic penalty is given by

$$E_{\rm del} = 2\int_0^{\ell/2}\left[\frac{B}{2}\left(\frac{d\phi_\alpha}{ds}\right)^2 + \frac{Y}{2}(\gamma_\alpha - 1)^2\right]ds. \quad (4)$$

In the adhered region, in addition to bending and stretching, there is an energetic cost due to deformation of the substrate and due to the adhesive interactions of the sheet with the substrate. Therefore, this energy is given by,

$$E_{\rm adh} = 2\int_{\ell/2}^{L/2}\left[\frac{B}{2}\left(\frac{d\phi_\beta}{ds}\right)^2 + \frac{Y}{2}(\gamma_\beta - 1)^2 + e_{\rm sub}(h_\beta,\phi_\beta) - w_{\rm ad}\right]ds, \quad (5)$$

where $e_{\rm sub}(h_\beta,\phi_\beta)$ is the energy of the substrate. Although in the main text we consider a Winkler foundation, $e_{\rm sub} = (K/2)h_\beta^2$, this formulation also applies to a fluid substrate under some modifications that are worked out in Appendix A. The main difference between the two substrates is that while a Winkler foundation exerts forces only in the vertical direction (y axis), the fluid hydrostatic pressure is directed normal to the sheet. We emphasize that these foundations differ significantly from a solid-compliant substrate, which is frequently considered in the literature [26,43–48]. While a solid-compliant substrate accumulates energy under the blister due to compression, the Winkler and fluid surfaces remain undeformed in the delaminated section.

The last term in the integral of Eq. (5) refers to the adhesion energy, $w_{\rm ad}$. This term is a constant that represents the work per undeformed unit area that is required to separate two close by surfaces. The forces that bond the two surfaces together originate from short-range interactions between molecules of the sheet and the substrate that are in contact on the interface. Methods for measuring this constant can be found in Refs. [21,22,49]. In the case of a solid that is lying on a fluid substrate, this term accounts for the interfacial toughness [25,34].

To obtain the equations for the equilibrium structure of the film, we must minimize $G = E - P\Delta$ given the geometric constraint, Eq. (1). For this purpose, we first normalize all lengths by the length-scale of the wrinkles: $\ell_w = (B/K)^{1/4}$ (for example $s \to s/\ell_w$). This length-scale does not depend on the blister phenomena and is manifest as the wavelength of the wrinkling pattern in a completely adhered sheet [28,50]. In addition, the total energy is rescaled by B/ℓ_w; and accordingly, the pressure and the adhesion are rescaled by $(BK)^{1/2}$. Second, we express the displacement as a function of our fields [9,30],

$$\Delta = \int_{-L/2}^{L/2}(1 - \gamma\cos\phi)ds = 2\int_0^{\ell/2}(1-\gamma_\alpha\cos\phi_\alpha)ds + 2\int_{\ell/2}^{L/2}(1-\gamma_\beta\cos\phi_\beta)ds, \quad (6)$$

and write the total energy as $G = 2\int_0^{\ell/2}\mathcal{L}_1 ds + 2\int_{\ell/2}^{L/2}\mathcal{L}_2 ds$, where

$$\mathcal{L}_1 = \frac{1}{2}\left(\frac{d\phi_\alpha}{ds}\right)^2 + \frac{1}{2\xi}(\gamma_\alpha - 1)^2 - P(1-\gamma_\alpha\cos\phi_\alpha) - Q_\alpha\left(\gamma_\alpha\sin\phi_\alpha - \frac{dh_\alpha}{ds}\right), \quad (7a)$$

$$\mathcal{L}_2 = \frac{1}{2}\left(\frac{d\phi_\beta}{ds}\right)^2 + \frac{1}{2\xi}(\gamma_\beta - 1)^2 + e_{\rm sub} - w_{\rm ad} - P(1-\gamma_\beta\cos\phi_\beta) - Q_\beta\left(\gamma_\beta\sin\phi_\beta - \frac{dh_\beta}{ds}\right). \quad (7b)$$

In the above expressions, Q_i ($i = \alpha,\beta$) are Lagrange multipliers that enforce the geometric constraint, Eq. (1), in each regime and $1/\xi = Y\ell_w^2/B \propto t^{-1/2}$ is a dimensionless parameter that measures the degree of extensibility; when $\xi \to 0$, the sheet becomes inextensible since the energetic cost for stretching diverges. Initially, the problem was characterized by five independent constants: B, Y, L, K and $w_{\rm ad}$. Because the energy is arbitrarily rescaled by B/ℓ_w, we are left with only four independent length-scales: the rest length L, the thickness $t = (B/Y)^{1/2}$, the capillary length, $\ell_c = (w_{\rm ad}/K)^{1/2}$, and the elastocapillary length, $\ell_{\rm ec} = (B/w_{\rm ad})^{1/2}$. Note that ℓ_w depends on the last two by $\ell_w = (\ell_c\ell_{\rm ec})^{1/2}$.

Finally, minimization of Eq. (7a) with respect to $\phi_\alpha, \gamma_\alpha, Q_\alpha$, and h_α yield the following equilibrium equations (see Appendix B for details):

$$0 = \frac{d^2\phi_\alpha}{ds^2} + P\gamma_\alpha\sin\phi_\alpha + Q_\alpha\gamma_\alpha\cos\phi_\alpha, \quad (8a)$$

$$0 = \frac{1}{\xi}(\gamma_\alpha - 1) + P\cos\phi_\alpha - Q_\alpha\sin\phi_\alpha, \quad (8b)$$

$$0 = \frac{dh_\alpha}{ds} - \gamma_\alpha\sin\phi_\alpha, \quad (8c)$$

$$0 = \frac{dQ_\alpha}{ds}, \quad (8d)$$

and similarly, minimization of Eq. (7b) with respect to the β-fields gives

$$0 = \frac{d^2\phi_\beta}{ds^2} + P\gamma_\beta\sin\phi_\beta + Q_\beta\gamma_\beta\cos\phi_\beta, \quad (9a)$$

$$0 = \frac{1}{\xi}(\gamma_\beta - 1) + P\cos\phi_\beta - Q_\beta\sin\phi_\beta, \quad (9b)$$

$$0 = \frac{dh_\beta}{ds} - \gamma_\beta \sin\phi_\beta, \tag{9c}$$

$$0 = \frac{de_{\rm sub}}{dh_\beta} - \frac{dQ_\beta}{ds}. \tag{9d}$$

While Eqs. (8a) and (9a) describe the balance of normal forces on a finite segment of the sheet, Eqs. (8b) and (9b) describe the balance of forces in the tangential direction. In addition, by Eq. (9d), the Lagrange multiplier, Q_β, is the total vertical force that the substrate exerts on the sheet up to a point s in the adhered section, $Q_\beta = \int_s^{L/2} h_\beta ds$. Similarly, Q_α accounts for the vertical force that acts on the edge of the delaminated portion of the sheet, $s = \ell/2$.

Equations (8) and (9) form a system of eight differential equations. To close the system, nine boundary conditions must be provided [51]. First, the even symmetry of the profile implies

$$\phi_\alpha(0) = 0. \tag{10}$$

Second, two boundary conditions are required at the sheet end, $s = L/2$. In this derivation, we assume the following hinged boundary conditions:

$$h_\beta(L/2) = 0, \tag{11a}$$

$$\frac{d\phi_\beta}{ds}(L/2) = 0. \tag{11b}$$

Third, we demand that the height function and the angle field will be continuous over the point of delamination,

$$h_\alpha(\ell/2) = h_\beta(\ell/2), \tag{12a}$$

$$\phi_\alpha(\ell/2) = \phi_\beta(\ell/2). \tag{12b}$$

Fourth, following the procedure in Appendix B, we obtain three natural conditions for the minimizing configuration,

$$0 = \left[\frac{d\phi_\alpha}{ds} - \frac{d\phi_\beta}{ds}\right]_{s=\frac{\ell}{2}}, \tag{13a}$$

$$0 = Q_\beta(\ell/2), \tag{13b}$$

$$0 = Q_\alpha(0), \tag{13c}$$

Equation (13a) guarantees the continuity of the bending moments, $M_i = d\phi_i/ds$ ($i = \alpha,\beta$), at $s = \ell/2$. In addition, since the sheet is confined only by the horizontal force, P, and no vertical force (or vertical displacement) is prescribed at the boundaries, the total force from the substrate in the y direction must vanish. This requirement is specified by Eq. (13b), $Q_\beta(\ell/2) = \int_{\ell/2}^{L/2} h_\beta ds = 0$. Last, the even symmetry of the solution implies Eq. (13c); when $Q_\alpha(0) = 0$, we have from Eqs. (8a) and (10) that the bending moment is maximum at the center of the sheet, i.e., $(dM_\alpha/ds)_{s=0} \equiv (d^2\phi_\alpha/ds^2)_{s=0} = 0$, as required by the even symmetry of the solution. We note that the continuity of ϕ and h, Eq. (12), along with the latter boundary conditions, imply the continuity of the compression field, γ. Thus, the tangential force, $\sigma^i_{\rm ss} = (\gamma_i - 1)/\xi$, and the normal force, $\sigma^i_{\rm sn} = (1/\gamma)d^2\phi/d^2s$, are both continuous at the point of delamination.

The last boundary condition is obtained by minimization of the total energy with respect to ℓ [13,21,34,36–38,52]. This condition is equivalent to Griffith's theorem, which relates the interfacial toughness of the material to the energy release rate [20,37]. We derive this boundary condition explicitly in Appendix B 1. The result of this minimization fixes the height of the sheet at the point of delamination,

$$h_\beta(\ell/2) = (2w_{\rm ad})^{1/2}. \tag{14}$$

The above discussion completes the formulation. In summary, given $L, \xi, w_{\rm ad}$, and P, one in principle can solve Eqs. (8) and (9) given the boundary conditions, Eqs. (10)–(14). In the next section, we derive an approximate nonlinear solution that captures the main physical essence of the system.

III. APPROXIMATE NONLINEAR SOLUTION FOR BLISTER FORMATION

In this section, we seek an approximate solution that is based on the following assumptions. (i) The total relaxed length is long compare to any other length-scale in the system, $L \gg 1$. Thus, terms of order $1/L$ are neglected. (ii) Extensibility corrections are small, $\xi \ll 1$, and can be neglected. Yet, terms of order ξL are kept intact. This approximation was shown to be sufficient in the analysis of linear stability in other closely related problems [53,54]. (iii) The adhesion energy is small, $w_{\rm ad} \ll 1$. This assumption has two implications. First, since by definition the rescaled adhesion energy is given by $w_{\rm ad} = \ell_c/\ell_{\rm ec}$, the following scale separation must hold:

$$\ell_c \ll \ell_{\rm ec} \ll L. \tag{15}$$

Second, since $h_\beta(\ell/2) = \sqrt{2}\ell_c$ is small [see Eq. (14)] and we anticipate a decaying profile, the β fields can be approximated by their linear order. The α fields, however, may in general be large and go beyond this order.

Assumption (ii) and Eqs. (8b) and (9b) imply that the compression fields are given by

$$\gamma \equiv \gamma_i = 1 - \xi P. \tag{16}$$

In addition, utilizing assumption (iii) simplifies Eqs. (8) and (9) into

$$0 = \frac{d^2\phi_\alpha}{ds^2} + P\sin\phi_\alpha, \tag{17a}$$

$$0 = \sin\phi_\alpha - \frac{dh_\alpha}{ds}, \tag{17b}$$

$$0 = \frac{d^4h_\beta}{ds^4} + P\frac{d^2h_\beta}{ds^2} + h_\beta, \tag{17c}$$

where we used Eq. (8d) and the boundary condition, Eq. (13c), to set $Q_\alpha = 0$.

The solution of these equations is given by

$$\phi_\alpha(s) = 2\arcsin[m\ {\rm sn}(q(s+s_0),m^2)], \tag{18a}$$

$$h_\alpha(s) = h_0 + \frac{2m}{q}{\rm cn}[q(s+s_0),m^2], \tag{18b}$$

$$h_\beta(s) = e^{-\kappa\zeta}[B_1\cos(k\zeta) + B_2\sin(k\zeta)] + e^{\kappa\zeta}[B_3\cos(k\zeta) + B_4\sin(k\zeta)], \tag{18c}$$

where $\zeta = s - \ell/2$ and hereafter we use the conventional symbols for the various elliptic functions, sn, cn, $\mathcal{E}$, K, cn, sc, and $\rm sc^{-1}$, as defined in Ref. [55]. In addition, the wave

numbers, q and k, and the decay parameter, κ, are related to the pressure by

$$q = P^{1/2}, \tag{19a}$$
$$k = \tfrac{1}{2}(2+P)^{1/2}, \tag{19b}$$
$$\kappa = \tfrac{1}{2}(2-P)^{1/2}. \tag{19c}$$

Equations (18) introduce eight constants, $\{m,s_0,h_0,\ell,B_j\}$, that are yet to be determined by the boundary conditions. By assumption (i), we can readily eliminate two, $B_3 = B_4 = 0$. These constants corresponds to the boundary conditions at the sheet end, Eqs. (11). Since we anticipate a decaying profile far away from the centered blister, the correction from the boundary can be assumed smaller then $1/L$. Note that this assumption breaks down if $\kappa \ll 1$ such that $\kappa L \sim O(1)$ [29,56]. Thus, for the rest of this solution, we require that the pressure is below its maximum value, $P_{\max} = 2$.

Solving for the other six unknown constants using Eqs. (10) and (12)–(14) gives

$$s_0 = 0, \tag{20a}$$
$$h_0 = (2w_{\rm ad})^{1/2} - \frac{2m}{q}\mathrm{cn}(q\ell/2,m^2), \tag{20b}$$
$$B_1 = -\frac{k}{\kappa}B_2 = (2w_{\rm ad})^{1/2}, \tag{20c}$$
$$m\ \mathrm{sn}(q\ell/2,m^2) = \sin(B_1\kappa) \simeq B_1\kappa, \tag{20d}$$
$$m\ \mathrm{cn}(q\ell/2,m^2) = B_1\frac{k^2-3\kappa^2}{2q}, \tag{20e}$$

where in Eq. (20d) we expanded the right-hand side to leading order in B_1 as required by assumption (iii). Given the identity $\mathrm{sn}^2(x,m^2)+\mathrm{cn}^2(x,m^2)=1$, the last two equations, Eqs. (20d) and (20e), can be solved explicitly for the modulus m and the extent length ℓ. The solution reads

$$m = (w_{\rm ad}/2P)^{1/2}, \tag{21a}$$
$$\ell = \frac{2}{\sqrt{P}}\mathrm{cn}^{-1}(P-1,m^2), \tag{21b}$$

where to simplify the resulting expressions, we used Eqs. (19) and (20c) and the identity, $\mathrm{sc}^{-1}(\frac{[P(2-P)]^{1/2}}{P-1},m^2) = \mathrm{cn}^{-1}(P-1,m^2)$. Equations (21) is one of our central results; it relates the blister length to the applied pressure and the adhesion energy.

Equations (18)–(21) complete our approximated solution. In summary, given ξ, L, $w_{\rm ad}$, and the external pressure, P, the shape of the sheet on the xy plane is given by $\mathbf{r} = (x(s),h(s))$. In the delaminated regime, $0 < s < \ell/2$, we have the following nonlinear solution:

$$x_\alpha(s) = -s + \frac{2}{q}\mathcal{E}(qs,m^2), \tag{22a}$$
$$h_\alpha(s) = \frac{(2w_{\rm ad})^{1/2}}{P}[1+\mathrm{cn}(qs,m^2)], \tag{22b}$$

where we used Eqs. (20b) and (20e) to simplify Eq. (22b), and in the adhered regime, $\ell/2 < s < L/2$, the solution is given to linear order by

$$x_\beta(s) = (s-\ell/2) + x_\alpha(\ell/2), \tag{23a}$$
$$h_\beta(s) = \frac{(2w_{\rm ad})^{1/2}}{k}e^{-\kappa\zeta}\cos(k\zeta+\phi), \quad \tan\phi = \frac{\kappa}{k}. \tag{23b}$$

In these equations, x_α and x_β are calculated from Eq. (2a) in their respective level of approximation. In addition, it should be understood that the profiles at $s < 0$ are obtained by mirror symmetry around the y axis. In Fig. 2 we plot these height profiles for several values of the pressure, P, and compare the analytical profiles to the numerical solution of Eqs. (8) and (9). The agreement between the two validates our approximated solution to the problem.

Two comments should be added to the above solution. First, since the modulus of the elliptic functions is bounded between $0 \leqslant m \leqslant 1$ and the pressure is bounded from above by $P_{\max} = 2$, we find from Eq. (21a) that

$$m \in \left[w_{\rm ad}^{1/2}/2, 1\right], \tag{24a}$$
$$P \in [w_{\rm ad}/2, 2]. \tag{24b}$$

In addition, the fact that m does not approach continuously to zero is a mark of the first order adhered-to-blister transition as we further discuss in Sec. IV. Second, the maximum height of the blister,

$$A_{\max} \equiv h_\alpha(0) = \frac{(8w_{\rm ad})^{1/2}}{P}, \tag{25}$$

is independent of the modulus, m. Consequently, this expression holds for small ($m \ll 1$), as well as for large ($m \sim 1$) blisters.

A. Energy and pressure-displacement relation

To obtain the total energy, E, and the pressure-displacement relation, $\Delta(P)$, we substitute the solution, Eqs. (22) and (23), into Eqs. (3) and (6) and integrate. This gives,

$$E - E_0 = \frac{\xi L P^2}{2} + 2q^2\ell(m^2-1) + 4q\mathcal{E}(q\ell/2,m^2) + \frac{w_{\rm ad}}{2\kappa}(k^4+1-2k^2\kappa^2+13\kappa^4) + \ell w_{\rm ad}, \tag{26a}$$
$$\Delta = \xi L P + 2\ell - \frac{4}{q}\mathcal{E}(q\ell/2,m^2) + \frac{w_{\rm ad}}{2\kappa}(k^2+5\kappa^2), \tag{26b}$$

where $E_0 = -w_{\rm ad}L$ is the energy of the relaxed configuration and ℓ is given by Eq. (21b).

Investigation of Eq. (26b) indicates that the displacement, Δ, is a nonmonotonic function of the pressure, P. In Fig. 2, we plot several scenarios of this behavior. Increasing the displacement up to $\Delta = \Delta_{\min}(P_{\min})$, we find that there is no solution to the pressure-displacement relation. This means that the branch of the blister solutions to Eqs. (8) and (9) become available only at a finite confinement. This finite confinement increases with the adhesion energy [see Fig. 2(b)]. Thus, up to $\Delta_{\min}$, only adhered solutions, such as flat and wrinkles, are physically accessible and no delamination can occur. At $\Delta_{\min}$, the blister solutions become available, yet, they do not

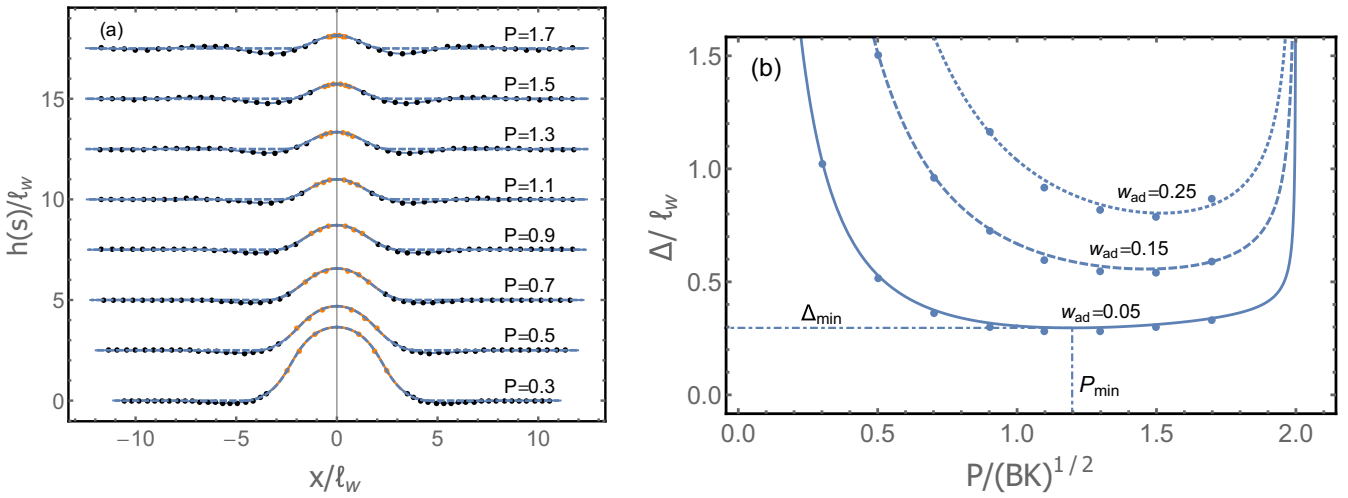

FIG. 2. Plots of the sheet configuration and the pressure-displacement relation for $L = 8\pi$ and $\xi = 0.005$. In panel (a), we plot the height function for several values of the pressure P and $w_{ad} = 0.15$. For clarity, the profiles are shifted along the y direction. In each configuration, the orange line marks the delaminated part of the sheet, Eqs. (22), the solid blue line marks the adhered oscillatory decay solution, Eqs. (23). In addition, the dashed blue line marks the blister solution on a rigid substrate; see Eqs. (34) in Sec. V. While at high pressures there are some deviations between the two solutions, they progressively converge at small pressures. The orange and black dots on each curve mark the numerical solution of Eqs. (8) and (9), respectively. (b) Plot of the pressure-displacement relation, Eq. (26b), for several values of w_{ad}, again the dots on each curve are evaluated numerically at the values of the pressure that are considered in panel (a). Note that all curves are non monotonic. For example, at the lowest adhesion energy, $w_{ad} = 0.05$, up to $\Delta_{min} \simeq 0.29$ ($P_{min} \simeq 1.19$) there is no solution to Eq. (26b); for $\Delta > \Delta_{min}$, there are two possible solutions, one with increasing pressure and therefore decreasing amplitude [see Eq. (25)] and second with decreasing pressure and therefore with increasing amplitude. The latter solution is the physical one as it has the lowest energy.

necessarily yield the minimum of the energy. At a given confinement the actual equilibrium configuration is always selected among all possible solutions, blistered and adhered, such as to minimize the total energy.

Beyond this minimum point, $\Delta > \Delta_{min}$, there exist two blistered solutions. One with decreasing pressure and therefore with increasing amplitude [see Eq. (25)], and second with increasing pressure and therefore with decreasing amplitude. As can be shown by direct substitution into the energy, Eq. (26a), the first solution is energetically favorable over the second one. Thus, from here on, we refer to the first blister solution as the one that is physically accessible. We note that this subtle, nonmonotonic behavior of the pressure-displacement relation has already been observed in other closely related systems [33,57,58].

IV. PATTERN TRANSITIONS FROM AN ADHERED SHEET TO A SMALL BLISTER

A thin elastic sheet that is adhered to a soft substrate and uniaxially compressed presents transitions between several morphologies [28]. Particularly, up to a critical confinement $\Delta_w \simeq 2\xi L$, the sheet remains flat and absorbs all the external pressure by in-plane stretching. Beyond this critical confinement, regular undulations (called wrinkles) with a well-defined wavelength, $\lambda = 2\pi\ell_w$, appears on the surface. The amplitude of the wrinkles' growth remains stable up to $\Delta_F \simeq \Delta_w + \lambda^2/L$. From there on, a localized pattern (fold) takes place [29,53,56]. In this section, we utilize the approximated solution to analyze the formation of a small blister from the flat or wrinkled states (see Fig. 1) as our goal is to derive the "phase-diagram" of the system [59].

A transition to a blistered state occurs when it is energetically preferable over the adhered solution. To analyze this transition, we first choose the displacement, Δ, and the maximum height, A_{max}, as the respective control and order parameters. Second, we assume that the two transitions occur at small enough confinements such that the blister can be estimated by its linear form, $m \ll 1$, Eq. (21a). Expanding the energy and the pressure-displacement relation, Eqs. (26), to leading order in m gives

$$E - E_0 \simeq \frac{\xi L P^2}{2} + \frac{w_{ad}}{\kappa}\left(1 + \frac{3}{2}\kappa\ell\right), \tag{27a}$$

$$\Delta \simeq \xi L P + \frac{1 + \kappa\ell/2}{\kappa P} w_{ad}, \tag{27b}$$

where the extent length ℓ, Eq. (21b), in this approximation is given by

$$\ell \simeq \frac{2}{\sqrt{P}} \cos^{-1}(P - 1). \tag{28}$$

Third, we derive the energies of the flat and wrinkled states [53],

$$E_f - E_0 = \frac{\Delta_f^2}{2\xi L}, \tag{29a}$$

$$E_W - E_0 \simeq 2\xi L + 2(\Delta_W - \Delta_w) + O((\Delta_W - \Delta_w)^2/L), \tag{29b}$$

where we use the subscripts "f" and "W" to denote the energies and the displacements of the flat and wrinkled states.

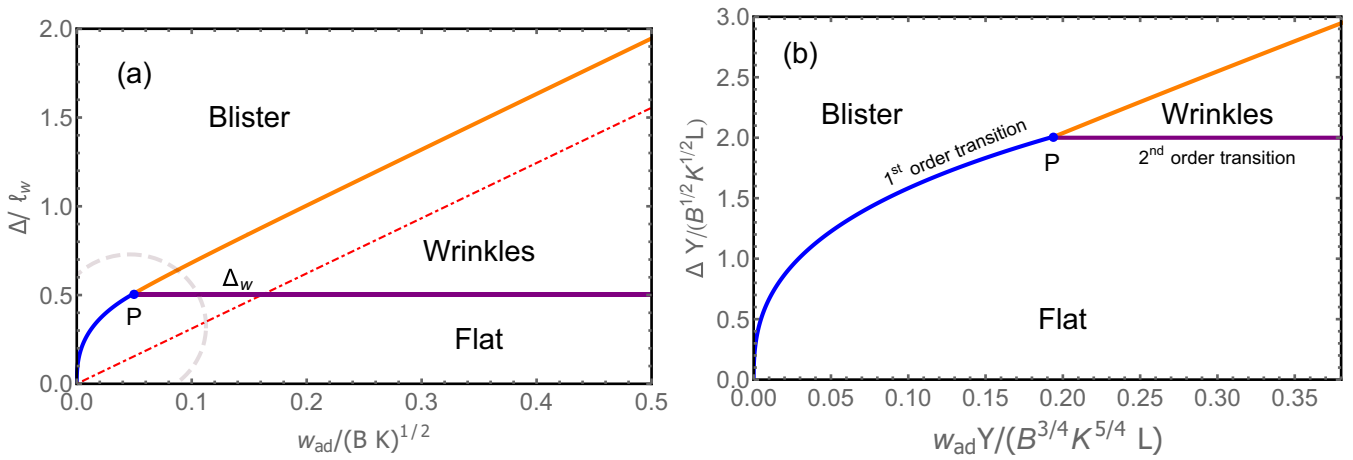

FIG. 3. (a) Phase diagram on $(w_{ad}/(BK)^{1/2}, \Delta/\ell_w)$ plane. In this diagram $\xi = 0.01$ and $L = 8\pi$ such that the flat-to-wrinkles displacement is $\Delta_w = 2\xi L \simeq 0.5$ (purple). Since the fold-to-blister transition was not analyzed in the present study, we cut the y axis at the critical wrinkles-to-fold displacement, $\Delta_F = \Delta_w + 4\pi^2/L \simeq 2.0$. The flat-to-blister, Eq. (30), and the wrinkles-to-blister, Eqs. (31), transitions are plotted respectively by the blue and orange lines. In the inextensible limit, $\xi \to 0$, the flat state diminishes as the triplet point, P, tends toward the origin of the diagram. In this limit the extensible wrinkles-to-blister displacement (orange) coincides with the inextensible prediction (dot-dashed red line), Eq. (32). (b) The phase diagram close to the triplet point [zoom-in the dashed circle from panel (a)]. For clarity, in this diagram we normalize the axes by ξL, i.e., consider $(w_{ad}/(\xi L), \Delta/(\xi L))$ plane. However, the axes labels in this diagram are obtained after dimensions are retrieved into these variables. As seen by Eqs. (30) and (31) under this normalization, the diagram becomes parameter free, i.e., independent on the specific values of ξ and L. Thus, in general the flat-to-blister transition occurs when $w_{ad}/(\xi L) \lesssim 0.2$. In addition, while the flat-to-wrinkles transition (purple) is of second order, the flat-to-blister and the wrinkles-to-blister transitions (blue and orange) marks a first-order transition.

To find the critical flat-to-blister displacement, we equate Eqs. (27a) and (29a) at a given displacement, $\Delta_f = \Delta$. This yields the parametric solution,

$$w_{ad} = \frac{2\ell\kappa^2 P^2}{(1+\kappa\ell/2)^2}\xi L, \tag{30a}$$

$$\Delta_{fb} = \xi L P + \frac{2\ell\kappa P}{1+\kappa\ell/2}\xi L, \tag{30b}$$

where Δ_{fb} is the flat-to-blister critical displacement. For a given w_{ad}, ξ, and L, we can solve Eq. (30a) for P and substitute in Eq. (30b) to obtain the critical flat-to-blister displacement. We cut this line at $\Delta_w = 2\xi L$, as in this displacement the flat state becomes unstable against the wrinkling. Thus, beyond Δ_w a transition to a blistered state, if it occurs, is initiated from a wrinkled pattern.

To analyze the latter transition, we equate Eqs. (27a) and (29b) and substitute $\Delta_W = \Delta$. This gives the parametric solution of the wrinkles-to-blister line,

$$w_{ad} = \frac{\kappa P(2-P)^2}{2(2-P)(1+\kappa\ell/2) - 2\kappa P\ell}\xi L, \tag{31a}$$

$$\Delta_{wb} = \frac{(4-P^2)(1+\kappa\ell/2) - 2P^2\kappa\ell}{2(2-P)(1+\kappa\ell/2) - 2\kappa P\ell}\xi L, \tag{31b}$$

where Δ_{wb} is the wrinkles-to-blister critical displacement.

In Fig. 3, we plot the phase diagram of the system as it is obtained from Eqs. (30) and (31). Two comments should be added regarding this diagram. First, although the transition from flat-to-wrinkles is of second order [53], the two transitions to a blistered state are always of a first order, i.e., the first derivative of the energy, $P = dE/d\Delta$, is discontinuous at the transition. Since P is finite at the transition, the order parameter $A_{max} = (8w_{ad})^{1/2}/P$ jumps from zero to a finite value. Experimentally, this first-order transition will be manifested by a hysteresis behavior of the amplitude. Although the amplitude behaves discontinuously at the adhered-to-blister transitions, it is expected to behave continuously in the opposite, blister-to-adhere, route. This is because the energy release rate, Eq. (14), acts to set an energetic barrier in the former case, but it has no effect on the latter case, which involves reformation of adhesive interactions.

Second, since practically extensibility corrections are very small, it is useful to consider the inextensible limit, $\xi \to 0$, of the above predictions. In this limit, the flat state diminishes and only the wrinkles-to-blister transition is considered. To obtain the critical displacement of this transition, we first set $\xi = 0$ in Eqs. (27) and (29b). Next, we equate the resulting energies, $E = E_W$, at a given displacement; this gives, $P \simeq 1.12$. Finally, we substitute this pressure back into Eq. (27b) and extract the critical displacement,

$$\Delta_{wb} \simeq 3.11 w_{ad}. \tag{32}$$

This result is plotted in the phase-diagram, Fig. 3(a). Taking the limit $\xi \to 0$ in this diagram is equivalent to shifting the point P toward the origin. In this limiting case, the line that is predicted by Eq. (31) will coincide with Eq. (32). In addition, since in the inextensible case wrinkles become unstable against folding at $\Delta_F = 4\pi^2/L$ [56], a wrinkles-to-blister transition will only occur if $\Delta_{wb} < \Delta_F$, i.e., $w_{ad} \lesssim 12.7/L$.

V. FORMATION OF A BOUNDARY LAYER AT THE EDGE OF A LARGE BLISTER

In this section, we show that our approximated solution converges to the known solution of a blister on a rigid substrate [34] for large enough confinements, i.e., small pressure $P \sim w_{\rm ad}$. This convergence marks the formation of a boundary layer at the vicinity of delamination.

To adapt the present model to the case of a rigid substrate, we first set $h^r_\beta(s) = \phi^r_\beta(s) = 0$, such that Eqs. (9) are automatically satisfied and $\gamma^r_\beta = \gamma$. To differentiate the current solution from the previous one, we denote the rigid substrate fields by superscript or subscript r. Second, we impose the following boundary conditions on Eqs. (8),

$$\phi^r_\alpha(0) = Q^r_\alpha(0) = \phi^r_\alpha(\ell/2) = h^r_\alpha(\ell/2) = 0, \tag{33a}$$

$$M_r = (2w_{\rm ad})^{1/2}, \tag{33b}$$

where $M_r = (d\phi^r_\alpha/ds)_{s=\ell/2}$ is the bending moment at $s = \ell/2$. These boundary conditions are obtained by similar methods as we describe in Sec. II and Appendix B. Third, we reduce Eqs. (8) to their approximated form, Eqs. (17), and solve them given the boundary conditions, Eqs. (33). The solution reads

$$h^r_\alpha = \frac{(2w_{\rm ad})^{1/2}}{P}\left[1 + \mathrm{cn}\left(qs, m_r^2\right)\right], \tag{34a}$$

$$m_r = \sqrt{\frac{w_{\rm ad}}{2P}}, \tag{34b}$$

$$\ell_r = \frac{4\mathrm{K}\left(m_r^2\right)}{\sqrt{P}}. \tag{34c}$$

Before we compare this solution with the one that we have obtained for a soft substrate, we emphasize their main differences in the following three points. (i) While Eq. (14) states that the work of adhesion is balanced by the energy of the substrate, Eq. (33b) states that adhesion is balanced by the work of the bending moment. (ii) When dimensions are retrieved into these equations, we find that while Eq. (14) gives rise to the capillary length-scale, ℓ_c, the latter, Eq. (33b), introduces the elastocapillary length-scale, $\ell_{\rm ec}$. In fact, in the case of a rigid substrate $K \to \infty$, the length-scales ℓ_w and ℓ_c are completely suppressed [60]. (iii) While for a rigid substrate the first derivative of ϕ is discontinuous at $s = \ell/2$ (discontinuous bending moment), in the current formulation discontinuity appears only at higher derivatives of ϕ; the first derivative of the angle must be continuous as dictated by Eq. (13a).

Despite these differences, the two models converge. Comparing Eqs. (34a) and Eq. (22b), we find that the solutions coincide given that the parameters, m_r and ℓ_r, coincide with their counterparts m and ℓ. From Eqs. (21b) and (34c) and the relation $\mathrm{cn}^{-1}(x \to -1, m^2) \to 2K(m^2)$, we find that $\ell \to \ell_r$ in the limit $P \ll 1$. Similarly, comparing Eqs. (21a) and (34b) we find, surprisingly, that $m_r = m$ independent of the value of the pressure. Thus, the solutions of the two models become equivalent for large enough confinements.

In Fig. 2, we plot the height profile on a rigid substrate, Eqs. (34), against the soft substrate one, Eqs. (22) and (23). While at high values of the pressures there are significant differences between the two, at small pressures, $P \sim w_{\rm ad}$, they converge up to vanishingly small deviations at the point of delamination.

This convergence marks the formation of a boundary layer at the point of delamination across which gradients of the bending moment rapidly decay to zero. To explore this layer, we first calculate the bending moment, $M_i = d\phi_i/ds$, in each regime,

$$M_\alpha = (2w_{\rm ad})^{1/2}\mathrm{cn}(qs, m^2), \tag{35a}$$

$$M_\beta = \frac{(2w_{\rm ad})^{1/2}}{k} e^{-\kappa\zeta}\left[2k\kappa\,\sin(k\zeta + \phi) - \frac{q^2}{2}\cos(k\zeta + \phi)\right], \tag{35b}$$

and then expand the resulting expressions around $s = \ell/2$,

$$M_i \simeq M_i(\ell/2) + \sigma^i_{\rm sn}(s - \ell/2) + \frac{d\sigma^i_{\rm sn}}{ds}(s - \ell/2)^2 + \cdots. \tag{36}$$

Keeping in mind our order of approximation, the various constants in this expansion reads

$$M_\alpha = M_\beta = (2w_{\rm ad})^{1/2}(1 - P), \tag{37a}$$

$$\sigma^\alpha_{\rm sn} = \sigma^\beta_{\rm sn} = (2w_{\rm ad})^{1/2}(2 - P)^{1/2}P, \tag{37b}$$

$$\frac{d\sigma^\alpha_{\rm sn}}{ds} = (w_{\rm ad}/2)^{1/2}(P - 1)P, \tag{37c}$$

$$\frac{d\sigma^\beta_{\rm sn}}{ds} = \frac{d\sigma^\alpha_{\rm sn}}{ds} - (w_{\rm ad}/2)^{1/2}. \tag{37d}$$

Since the boundary layer is created at large confinements, we restrict the following discussion to small values of $P \sim w_{\rm ad}$. From Eq. (37a), we see that the bending moment is continuous across $\ell/2$ and it approaches M_r from below as P diminishes, $M_i \to M_r \sim (2w_{\rm ad})^{1/2} \propto \ell_{\rm ec}^{-1}$. In the latter expression and in the subsequent ones, the proportionality is obtained after dimensions are retrieved from M_i/B. The first-order correction to the rigid substrate solution scales as $M_r - M_i \sim w_{\rm ad}^{3/2} \propto \ell_c/\ell_{\rm ec}^2$. Thus, in the limit of a rigid substrate, $K \to \infty$ and therefore $\ell_c \to 0$, this correction diminishes and the bending moment converges to a constant which is independent on the substrate stiffness.

The first derivative of the bending moment, the normal force $\sigma^i_{\rm sn}$, is also continuous across the point of delamination, Eq. (37b). The fact that this force diminishes at small pressures, $\sigma^i_{\rm sn} \sim w_{\rm ad}^{3/2} \propto \ell_c^{1/2}/\ell_{\rm ec}^{5/2}$, has two consequences, (i) the point $s = \ell/2$ becomes maximum of the bending moment, and (ii) the second derivative of the bending moment becomes the leading order correction in the expansion, Eq. (36). Thus, discontinuity first appears only in the second derivative of M_i (third derivative of ϕ). This order is beyond the continuity that is dictated by the force balance equations, Eqs. (8) and (9).

When we approach the take-off point from the left, $s \to (\ell/2)_-$, we find from Eq. (37c) that $d\sigma^\alpha_{\rm sn}/ds \sim w_{\rm ad}^{3/2} \propto \ell_{\rm ec}^{-3}$, while when we approach it from the right, $s \to (\ell/2)_+$, we find from Eq. (37d) that $d\sigma^\beta_{\rm sn}/ds \sim w_{\rm ad}^{1/2} \propto 1/(\ell_c\ell_{\rm ec}^2)$. Since

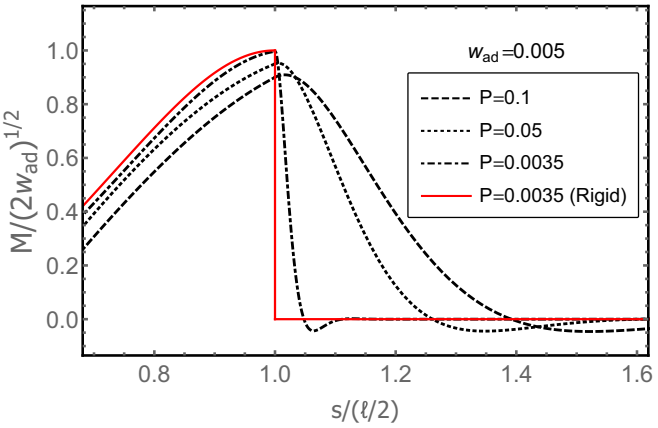

FIG. 4. The normalized bending moment at the edge of delamination as a function of the normalized coordinate $s/(\ell/2)$. In this plot, $w_{ad} = 0.005$ and three different pressures are considered, $P = 0.1, 0.05, 0.0035$. The red solid line marks the discontinuous solution of the bending moment on a rigid substrate. As the pressure decreases, the profiles converge to the discontinuous solution up to a narrow boundary layer of width w. Although the width of this layer remains constant, its relative length with respect to ℓ shrinks to zero.

$\ell_c \ll \ell_{ec}$ the gradients in the delaminated region are much smaller than in the adhered region. In fact, while the latter decay to zero over a distance $w \sim 1/\kappa \propto \ell_w$, the former decay to zero over much larger distance, $M_\alpha \simeq 0$ at $s \simeq \ell/4$ [see Eqs. (35a) and (21a)]. Thus, the width over which the profile decays to zero in the adhered region, w, relative to the delaminated extent length, $\ell \propto \ell_{ec}$, diminishes at large confinements, $w/\ell \sim (\ell_c/\ell_{ec})^{1/2} \ll 1$.

In Fig. 4, we plot Eqs. (35) for the bending moments as a function of the normalized coordinate, $u = s/(\ell/2)$. As the pressure drops, the relative gradients between the delaminated and the adhered regions grow such that ultimately sharp transition between the two regimes is obtained, as we would expect from a boundary layer.

VI. CONCLUSIONS

Inspired by efforts to remove biofilms from soft surfaces, we modeled the behavior of a thin sheet that is lying on top of a compliant substrate and is uniaxially compressed from the boundaries. Our aim was to determine the necessary displacement and pressure that causes a portion of the film to form a blister, which is delaminated from this surface. The formation of this blister facilitates the removal of the thin film from the surface and can thereby inhibit the fouling of the system. Moreover, by considering a soft surface, which is approximated by the Winkler model, we relaxed the assumption of a rigid substrate that was considered elsewhere [34,37].

Our formulation yields a closed system of differential equations and boundary conditions that describe the continuous force and moment balance transitions across the point of delamination. In particular, similar to the Jurins law [61] in capillary phenomenon, the height of the sheet at the point of delamination is determined by a balance between the substrate and adhesion energies, Eq. (14). This boundary condition links the elastic shape to the adhesion energy.

TABLE I. Summary of the main results.

Critical displacements of the pattern transitions		
	Extensible	Inextensible
Flat-to-blister, Δ_{fb}	Eq. (30)	Not applicable
Wrinkles-to-blister, Δ_{wb}	Eq. (31)	Eq. (32)
Main differences between blisters on soft and rigid substrates		
	Soft substrate	Rigid substrate
Height function $h(s)$	Eqs. (22) and (23)	Eq. (34a)
Energy release rate	Eq. (14)	Eq. (33b)
Blister length, ℓ	Eq. (21b)	Eq. (34c)
Maximum height, A_{max}	$(8w_{ad})^{1/2}/P$	$(8w_{ad})^{1/2}/P$

Under the set of assumptions that we postulated in Sec. III, we solved this system of equations. This solution conserves aspects of the inherent nonlinearity of the problem by allowing the height of the delaminated region to go beyond linear order. Two comments should be added to these assumptions. First, in our model, we have neglected the energy of the meniscus. This energy, which is associated with the shape of the substrate beneath the delaminated sheet, can be estimated by $E_m/(B/\ell_w) \simeq (B/\ell_w)\sqrt{w_{ad}K}\,\ell_c^2 = w_{ad}^{3/2}$ (see Appendix A in Ref. [19]), where E_m is the meniscus energy. Since this term is proportional to $w_{ad}^{3/2}$, it is negligible at our order of approximation. Second, we note that in the case of an inextensible sheet that is lying on a fluid substrate, each regime (delaminated and adhered) have exact solutions [9,54]; the challenge is, however, to combine the two solutions such that the boundary conditions are correctly satisfied.

We showed that this approximated solution converges to the known solution of a blister on a rigid substrate, for summary see Table I. Consequently, for sufficiently strong confinement, the elastic shape approximately satisfies the boundary condition of a discontinuous bending moment even for very soft foundations. This convergence can be rationalized quantitatively when the respective energies of the substrate and the blister are considered. In the limit of large confinements, the energy of the substrate and the blister scales as w_{ad} and $w_{ad}^{1/2}$, respectively [see the third and forth terms in Eq. (26a)]. Thus, when $w_{ad} \ll 1$, most of the energy is localized in the blister and only a small part of it is stored in the substrate. This approximates the rigid substrate scenario, which neglects the energy of the substrate altogether.

A surprising result that emerged from our studies is that the maximum heights of a blister on soft and rigid foundations are equal [compare Eqs. (25) and (34a) at $s = 0$]. Thus, even at small confinements, where we would expect large deviations due to the different boundary conditions of the two models, the two profiles agree up to some discrepancy at the blister edges. The latter discrepancy at the edges is due to different lengths for the extent of delamination in the two profiles, Eqs. (21b) and (34c). Our model provides details of the boundary layer that is forming on the substrate close to the critical point of delamination. We showed that the penetration length of this layer inside the substrate scales as $\ell_w = (\ell_c \ell_{ec})^{1/2}$, which is much smaller then the elastocapillary length, ℓ_{ec}, over which the blister evolves.

Our approximated solution was also utilized to analyze the possible transitions between two adhered solutions, flat and wrinkled, to a blistered state; for summary of these results see Table I. Our findings are summarized in the phase diagrams, Figs. 3. Two general conclusions can be drawn from these diagrams. First, a flat-to-blister transition occurs for large enough confinement if $\eta \equiv \frac{w_{ad}}{\xi L} \lesssim 0.2$, where the parameter η accounts for the ratio between the energy of adhesion and the stretching energy of the sheet. Retrieving dimensions into this parameter and reordering terms we obtain the following criterion:

$$\text{flat-to-blister criterion:} \quad w_{ad} \lesssim 0.2\frac{B^{3/4}K^{5/4}L}{Y}. \tag{38}$$

Second, when $\eta > 0.2$, a transition from an adhered state to a delaminated state is initiated from wrinkles or a fold. In the present study, we did not analyze the fold-to-blister transition and therefore the following conclusions hold for $\Delta_{wb} < \Delta_F$; the blister-to-wrinkles transition appears before the wrinkles-to-fold transition. In general, the maximum value of η for which a wrinkles-to-blister transition occurs depends on ξ. This maximum value can be calculated numerically by setting $\Delta_{wb} = \Delta_F$ in Eq. (31b), solving for P and substituting this pressure in Eq. (31a). However, since in many practical cases, the stretching energy of the sheet can be neglected, $\xi L \to 0$, the criterion for the wrinkles-to-blister transition can be well approximated by the inextensible limit $w_{ad} \lesssim 12.7/L$. Retrieving dimensions into the latter expression, we obtain our second general conclusion,

$$\text{wrinkles-to-blister criterion (inextensible):}$$
$$w_{ad} \lesssim 12.7\frac{B^{3/4}K^{1/4}}{L}. \tag{39}$$

Although the detailed predictions of our phase diagram still requires experimental verification, the above criteria can be tested against known experimental results in two cases. First, in Ref. [28] a polyester thin sheet ($E = 2.5$ GPa) of length $L \sim 6$ cm with thicknesses $t = 10$ μm was placed on a water substrate ($K = 10^4$ N/m^3) and uniaxially compressed. In this experiment, the sheet evolved into a localized-folded state and no delamination had been observed. To check that this is consistent with our theory, we first notice that the sheet can be treated as in the inextensible limit since $\xi L \sim 10^{-5}$. Second, we plug the experimental parameters into Eq. (39). This gives $12.7B^{3/4}K^{1/4}/L \sim 10^{-4}$ J/m^2 and $w_{ad} \sim 0.07$ J/m^2. Thus, consistent with these experiments, the adhesion energy is too strong and no delamination is predicted by the theory.

However, in Refs. [27,62] 0.6- to 1.6-mm-thick rubber sheets ($E \sim 220$ KPa) of length $L = 40$ cm was placed on potassium carbonate liquid ($K = 1.5 \times 10^4$ N/m^3 and $w_{ad} = 102$ Nm/m) and compressed uniaxially. The parameters in these experiments gives $\xi L \sim 0.1$ and therefore $\eta \sim 0.7$–2.5. Since $\eta > 0.2$, we first conclude that a flat-to-blister transition will not occur. Second, since the extensibility corrections are not negligible ($\xi L \nrightarrow 0$) we cannot use our inextensible criterion, Eq. (39). Thus, to obtain an appropriate criterion for the latter case, we must go back to Eqs. (31) and substitute $\Delta_{wb} = \Delta_w + 4\pi^2/L \sim 1.3$ in them and solve for η. This gives the upper bound $\eta_{cr} \sim 3.2$. Thus, our theory predicts a wrinkles-to-blister transition at $0.2 \lesssim \eta \lesssim 3.2$. Indeed, in the latter references, these transitions were reported. However, because of the large thickness of the rubber the elastogravity length-scale became dominant over the elastocapillary length scale and thus the delaminated state converged to the heavy-elastica solution, where gravity plays an essential role in the elastic shape, instead of the elastica solution as considered here. In general, we expect that the addition of gravity to the system will shift the lines in our phase diagrams upward, such that delamination will occur at larger displacements. This is because the sheet will need to overcome its own weight in addition to the adhesive interactions to delaminate from the substrate.

While the Winkler model is adequate to describe small deformations of soft substrates, such as fluid or shallow adhesive layers [63], its predictions are, in general, not applicable to more stiff substrates. This is because Winkler's model takes into consideration only part of the substrate's elastic energy, i.e., it considers only vertical deformations of its surface and neglects most of its in-plane compression. This unaccounted elastic energy may result in qualitative as well as quantitative changes of the observed patterns. Thus, our results do not apply to stiffer substrates that are compressed underneath the blister as, for example, in Ref. [47]. In these systems, delamination is driven by a different mechanism: the competition between the bending energy of the sheet and the elastic compression of the substrate underneath the blister. Thus, the Winkler model is insufficient to capture this effect. For example, in the case of stiffer substrates, the jump into a blistered state is of a completely localized nature as it is independent of the total length of the sheet. In addition, the latter systems evolve into a state of multiple blisters and as explained in Ref. [57], this state is energetically unfavorable in the present model.

A possible means of experimentally verifying the present results could be achieved through the procedure described in Ref. [34], where a blister state was initially assumed. In this experiment, a thin sheet was pressed against an adhesive substrate through its entire length, accept for some portion at the center. The system was then released until an equilibrium state was obtained. Following this procedure for the current system should give the height profile, Eq. (22b), in the blistered regime. Measuring the maximum height, Eq. (25), as a function of the external pressure can confirm the results of the present model. Once confirmed, this method can be used as an independent measurement of the adhesion energy in other similar experimental setups.

The present work can be extended in several directions; here, we mention three of them. First, one can consider the addition of time dependent forces to the system. This could be done, for example, by periodic excitations of the compressing force. At a critical frequency, when the system is at resonance, the film can potentially jump into a blistered state even before our static criterion is achieved. Second, to better mimic the behavior of biological tissues, the time dependence could be added by replacing the elastic sheet with a viscoelastic one. Third, in light of the present results, and especially the new boundary conditions that show a continuous convergence into the moment discontinuity, it would be interesting to obtain a similar set of equations for two or three-dimensional vesicles that are lying on an adhesive substrate [64,65].

ACKNOWLEDGMENTS

We thank Dominic Vella and Haim Diamant for helpful comments. A.C.B. gratefully acknowledges financial support from the ONR N00014-16-1-3111.

APPENDIX A: THE EQUILIBRIUM EQUATIONS IN THE CASE OF A FLUID SUBSTRATE

Since the hydrostatic pressure that the fluid exerts on the sheet is oriented in the normal direction it has, in general, nonzero projection along the x and y axes. Although the total pressure along the y axis must vanish, similar to Eq. (13b), the corresponding component along the x direction is not zero. This component of the pressure displace the edge of the delaminated section. Consequently, the energy of the fluid has two contributions $e_{\rm sub} = e^1_{\rm sub} + e^2_{\rm sub}$. One is the work to displace the fluid from zero to a certain height in the adhered region,

$$e^1_{\rm sub} = \frac{1}{2}\int_{\ell/2}^{L/2} \gamma_\beta h_\beta^2 \cos\phi_\beta ds, \tag{A1}$$

and second is to displace the delaminated section,

$$e^2_{\rm sub} = P_s \int_0^{\ell/2} (1-\gamma_\alpha \cos\phi_\alpha) ds, \tag{A2}$$

where

$$P_s = \int_{\ell/2}^{L/2} \gamma_\beta h_\beta \sin\phi_\beta ds = -\frac{h_\beta^2(\ell/2)}{2}, \tag{A3}$$

is the total pressure in the x direction that the fluid exerts at $s = \ell/2$. To derive Eq. (A3) we have used the boundary condition, $h_\beta(L/2) = 0$, and the geometric constraint, Eq.(1).

Replacing the term for the Winkler foundation by the above energies modify Eqs. (7) into

$$\mathcal{L}_1 = \frac{1}{2}\left(\frac{d\phi_\alpha}{ds}\right)^2 + \frac{1}{2\xi}(\gamma_\alpha - 1)^2 - P(1-\gamma_\alpha\cos\phi_\alpha) - Q_\alpha\left(\gamma_\alpha\sin\phi_\alpha - \frac{dh_\alpha}{ds}\right) + P_s(1-\gamma_\alpha\cos\phi_\alpha), \tag{A4a}$$

$$\mathcal{L}_2 = \frac{1}{2}\left(\frac{d\phi_\beta}{ds}\right)^2 + \frac{1}{2\xi}(\gamma_\beta - 1)^2 + \frac{1}{2}\gamma_\beta h_\beta^2\cos\phi_\beta - w_{\rm ad} - P(1-\gamma_\beta\cos\phi_\beta) - Q_\beta\left(\gamma_\beta\sin\phi_\beta - \frac{dh_\beta}{ds}\right). \tag{A4b}$$

Following Appendix B and minimizing Eq. (A4a) with respect to the α fields gives

$$0 = \frac{d^2\phi_\alpha}{ds^2} + (P-P_s)\gamma_\alpha\sin\phi_\alpha + Q_\alpha\gamma_\alpha\cos\phi_\alpha, \tag{A5a}$$

$$0 = \frac{1}{\xi}(\gamma_\alpha - 1) + (P-P_s)\cos\phi_\alpha - Q_\alpha\sin\phi_\alpha, \tag{A5b}$$

$$0 = \frac{dh_\alpha}{ds} - \gamma_\alpha\sin\phi_\alpha, \tag{A5c}$$

$$0 = \frac{dQ_\alpha}{ds}. \tag{A5d}$$

Similarly, minimization of Eq. (A4b) reads

$$0 = \frac{d^2\phi_\beta}{ds^2} + \left(P + \frac{h_\beta^2}{2}\right)\gamma_\beta\sin\phi_\beta + Q_\beta\gamma_\beta\cos\phi_\beta, \tag{A6a}$$

$$0 = \frac{1}{\xi}(\gamma_\beta - 1) + \left(P + \frac{h_\beta^2}{2}\right)\cos\phi_\beta - Q_\beta\sin\phi_\beta, \tag{A6b}$$

$$0 = \frac{dh_\beta}{ds} - \gamma_\beta\sin\phi_\beta, \tag{A6c}$$

$$0 = \frac{de_{\rm sub}}{dh_\beta} - \frac{dQ_\beta}{ds}. \tag{A6d}$$

Following our derivation of the boundary conditions, Eqs. (10)–(14), we find that they remain unchanged. Thus, from Eq. (14) we have that $P_s = -w_{\rm ad}$. In addition, comparing Eqs. (A5a) and (A6a) and Eqs. (A5b) and (A6b) we find that the normal and tangential forces transforms continuously at the point of delamination.

In Sec. III the approximated solution is based on the assumption that $w_{\rm ad} \ll 1$. As a result, for large values of the pressure, $P \gg w_{\rm ad}$, the terms that are akin to P_s in Eqs. (A5) and (A6) can be neglected and the solution remains unchanged. However, for smaller values of the pressure, $P \sim w_{\rm ad}$, this modification should be considered. In this case a plausible approximation would be to replace P by $P - P_s$. It is then easy to verify that at our level of approximation there are no qualitative differences between the two foundations.

APPENDIX B: DERIVATION OF THE EQUILIBRIUM EQUATIONS AND BOUNDARY CONDITIONS IN THE CASE OF A DEFORMABLE SUBSTRATE

In this Appendix we carry out the minimization that leads to Eqs. (8) and (9) and the boundary conditions, Eqs. (13). In addition, in the subsequent subsection we will derive the boundary condition, Eq. (14). Our goal is to minimize the energy $G = \int_0^{\ell/2}\mathcal{L}_\alpha ds + \int_{\ell/2}^{L/2}\mathcal{L}_\beta ds$, where $\mathcal{L}_\alpha$ and $\mathcal{L}_\beta$ are given by Eqs. (7a) and (7b).

We carry out the minimization with respect to ϕ_i, γ_i, h_i, and Q_i ($i = \alpha, \beta$) in the standard way. We consider a small perturbation over these variables, for example, $\phi \to \phi_i + \delta\phi_i$, and then expand to linear order in $\delta\phi_i$. This procedure gives

$$\delta G = \left[\frac{d\phi_\alpha}{ds}\delta\phi_\alpha\right]_{s=0}^{s=\ell/2} + \left[\frac{d\phi_\beta}{ds}\delta\phi_\beta\right]_{s=\ell/2}^{s=L/2} + [Q_\alpha\delta h_\alpha]_{s=0}^{s=\ell/2} + [Q_\beta\delta h_\beta]_{s=\ell/2}^{s=L/2} + \int_0^{\ell/2}\left[\frac{d}{ds}\left(\frac{\partial\mathcal{L}_\alpha}{\partial(dx_i/ds)}\right) - \frac{\partial\mathcal{L}_\alpha}{\partial x_i}\right]\delta x_i ds + \int_{\ell/2}^{L/2}\left[\frac{d}{ds}\left(\frac{\partial\mathcal{L}_\beta}{\partial(dy_i/ds)}\right) - \frac{\partial\mathcal{L}_\beta}{\partial y_i}\right]\delta y_i ds, \tag{B1}$$

where in the second line $x_i = \phi_\alpha, \gamma_\alpha, h_\alpha, Q_\alpha$ and $y_i = \phi_\beta, \gamma_\beta, h_\beta, Q_\beta$ and it should be understood that there is a summation over the indexes i. Equating to zero each of the integrand in the second line readily yields the equilibrium equations, Eqs. (8) and (9).

The first line in Eq. (B1) gives the boundary conditions, Eqs. (13). To reveal this result we first note that since $\phi_\alpha(0)$ and $h_\beta(L/2)$ are prescribed $\delta\phi_\alpha(0) = \delta h_\beta(L/2) = 0$. In addition, the continuity conditions at $s = \ell/2$, Eq. (12), gives $\delta\phi_\alpha(\ell/2) = \delta\phi_\beta(\ell/2)$ and $\delta h_\alpha(\ell/2) = \delta h_\beta(\ell/2)$. Thus, we are left with

$$\delta G = \left(\frac{d\phi_\alpha}{ds} - \frac{d\phi_\beta}{ds}\right)_{\ell/2} \delta\phi_\alpha(\ell/2) + \left(Q_\alpha - Q_\beta\right)_{s=\ell/2} \times \delta h_\alpha(\ell/2) - Q_\alpha(0)\delta h_\alpha(0), \tag{B2}$$

where $(d\phi_\beta/ds)_{s=\ell/2} = 0$ was used. Since $\delta\phi_\alpha(\ell/2)$, $\delta h_\alpha(\ell/2)$, and $\delta h_\alpha(0)$ are arbitrary, we can independently equate each of their coefficients to zero. This yields the boundary conditions, Eqs. (13).

Derivation of Eq. (14)

In this subsection, we elaborate on the boundary condition that is obtained by minimization of the total energy with respect to the delamination length, ℓ. Following Refs. [37,64,66,67] we minimize the energy, G, with respect to ℓ. This gives the following equation:

$$\frac{\delta G}{\delta \ell} = \frac{1}{2}\mathcal{L}_1(\ell/2) - \frac{1}{2}\mathcal{L}_2(\ell/2) + \left(\frac{d\phi_\alpha}{ds}\frac{d\phi_\alpha}{d\ell}\right)_{s=\ell/2} - \left(\frac{d\phi_\beta}{ds}\frac{d\phi_\beta}{d\ell}\right)_{s=\ell/2}, \tag{B3}$$

where to simplify the final result we have used Eqs. (8), (9), and (13). Equation (B3) can further be simplified using the following arguments. A small perturbation in the delamination length, $\ell \to \ell^\star + \delta\ell$, must yield a perturbation in the angles fields, $\phi_\alpha \to \phi_\alpha^\star + \delta\phi_\alpha$ and $\phi_\beta \to \phi_\beta^\star + \delta\phi_\beta$. Consequently, at $s = \ell/2$ these fields can be expanded as follows:

$$\phi_\alpha(\ell/2) = \phi_\alpha^\star[(\ell^\star + \delta\ell)/2] + \delta\phi_\alpha[(\ell^\star + \delta\ell)/2] \simeq \phi_\alpha^\star(\ell^\star/2) + \frac{1}{2}\left(\frac{d\phi_\alpha^\star}{ds}\right)_{s=\frac{\ell^\star}{2}} \delta\ell + \delta\phi_\alpha(\ell^\star/2), \tag{B4a}$$

$$\phi_\beta(\ell/2) = \phi_\beta^\star[(\ell^\star + \delta\ell)/2] + \delta\phi_\beta[(\ell^\star + \delta\ell)/2] \simeq \phi_\beta^\star(\ell^\star/2) + \frac{1}{2}\left(\frac{d\phi_\beta^\star}{ds}\right)_{s=\frac{\ell^\star}{2}} \delta\ell + \delta\phi_\beta(\ell^\star/2). \tag{B4b}$$

Subtracting the two equations and noting that by the continuity conditions, Eqs. (12), $\phi_\alpha(\ell/2) = \phi_\beta(\ell/2)$ and $\phi_\alpha^\star(\ell^\star/2) = \phi_\beta^\star(\ell^\star/2)$, we have

$$\frac{d\phi_\beta}{d\ell} - \frac{d\phi_\alpha}{d\ell} = \frac{1}{2}\left(\frac{d\phi_\alpha^\star}{ds} - \frac{d\phi_\beta^\star}{ds}\right) = 0, \tag{B5}$$

where we have used $\delta\phi_i/\delta\ell = d\phi_i/d\ell$. In addition, the last equality holds since the bending moment is continuous, Eq. (13a). Last, substituting Eqs. (B5) in (B3) and using Eqs. (7a) and (7b) gives

$$\frac{\delta G}{\delta \ell} = \frac{1}{2}(w_{\text{ad}} - e_{\text{sub}}). \tag{B6}$$

The boundary condition, Eq. (14), is obtained once we equate Eq. (B6) to zero.

[1] E. Cerda and L. Mahadevan, Phys. Rev. Lett. **90**, 074302 (2003).
[2] E. Cerda and L. Mahadevan, Phys. Rev. Lett. **80**, 2358 (1998).
[3] M. Marder, E. Sharon, S. Smith, and B. Roman, Europhys. Lett. **62**, 498 (2003).
[4] J. Dervaux, P. Ciarletta, and M. B. Amar, J. Mech. Phys. Solids **57**, 458 (2009).
[5] J. Huang, B. Davidovitch, C. D. Santangelo, T. P. Russell, and N. Menon, Phys. Rev. Lett. **105**, 038302 (2010).
[6] B. Davidovitch, R. D. Schroll, D. Vella, M. Adda-Bedia, and E. A. Cerda, Proc. Natl. Acad. Sci. USA **108**, 18227 (2011).
[7] B. Audoly, Phys. Rev. E **84**, 011605 (2011).
[8] F. Brau, P. Damman, H. Diamant, and T. A. Witten, Soft Matter **9**, 8177 (2013).
[9] H. Diamant and T. A. Witten, Phys. Rev. Lett. **107**, 164302 (2011).
[10] T. A. Witten, Rev. Mod. Phys. **79**, 643 (2007).
[11] H. King, R. D. Schroll, B. Davidovitch, and N. Menon, Proc. Natl. Acad. Sci. USA **109**, 9716 (2012).
[12] J. W. Hutchinson and Z. Suo, Adv. Appl. Mech. **29**, 63 (1991).
[13] B. Roman and J. Bico, J. Phys.: Condens. Matter **22**, 493101 (2010).
[14] M. Adda-Bedia and L. Mahadevan, Proc. R. Soc. A **462**, 3233 (2006).
[15] O. Kruglova, F. Brau, D. Villers, and P. Damman, Phys. Rev. Lett. **107**, 164303 (2011).
[16] F. Brau, Phys. Rev. E **90**, 062406 (2014).
[17] B. Roman, Int. J. Fract. **182**, 209 (2013).
[18] J. Hure, B. Roman, and J. Bico, Phys. Rev. Lett. **106**, 174301 (2011).
[19] E. Hohlfeld and B. Davidovitch, Phys. Rev. E **91**, 012407 (2015).
[20] C. T. Sun and Z.-H. Jin, *Fracture Mechanics* (Elsevier, New York, 2012).
[21] K. Kendall, *Molecular Adhesion and Its Applications: The Sticky Universe* (Kluwer Academic, Dordrecht, 2001).
[22] J. N. Israelachvili, *Intermolecular and Surface Forces*, 3rd ed. (Elsevier, 2011).
[23] G. Gioia and M. Ortiz (Elsevier, New York, 1997) pp. 119–192.
[24] B. Audoly, Phys. Rev. Lett. **83**, 4124 (1999).
[25] J. Chopin, D. Vella, and A. Boudaoud, Proc. R. Soc. London A **464**, 2887 (2008).
[26] M. A. Biot, J. Appl. Mech. **203** (1936).
[27] T. J. W. Wagner and D. Vella, Phys. Rev. Lett. **107**, 044301 (2011).
[28] L. Pocivavsek, R. Dellsy, A. Kern, S. Johnson, B. Lin, K. Y. C. Lee, and E. Cerda, Science **320**, 912 (2008).
[29] H. Diamant and T. A. Witten, arXiv:1009.2487.
[30] H. Diamant and T. A. Witten, Phys. Rev. E **88**, 012401 (2013).
[31] C. Wang, Int. J. Mech. Sci. **28**, 549 (1986).

[32] D. Vella, A. Boudaoud, and M. Adda-Bedia, Phys. Rev. Lett. **103**, 174301 (2009).
[33] A. A. Lee, C. L. Gouellec, and D. Vella, Extreme Mech. Lett. **5**, 81 (2015).
[34] T. J. W. Wagner and D. Vella, Soft Matter **9**, 1025 (2013).
[35] L. D. Landau and E. M. Lifshitz, *Theory of Elasticity*, 3rd ed. (Butterworth-Heinemann, Oxford, 1986).
[36] C. Majidi, Mech. Res. Commun. **34**, 85 (2007).
[37] C. Majidi and G. G. Adams, Proc. R. Soc. A **465**, 2217 (2009).
[38] N. J. Glassmaker and C. Y. Hui, J. Appl. Phys. **96**, 3429 (2004).
[39] J. W. Obreimoff, Proc. R. Soc. A **127**, 290 (1930).
[40] S. S. Branda, Åshild Vik, L. Friedman, and R. Kolter, Trends Microbiol. **13**, 20 (2005).
[41] A. Epstein, D. Hong, P. Kim, and J. Aizenberg, New J. Phys **15**, 095018 (2013).
[42] C. Zhang, B. Li, J.-Y. Tang, X.-L. Wang, Z. Qin, and X.-Q. Feng, Soft Matter **13**, 7389 (2017).
[43] H.-H. Yu and J. W. Hutchinson, Int. J. Fract. **113**, 39 (2002).
[44] G. Parry, J. Colin, C. Coupeau, F. Foucher, A. Cimetière, and J. Grilhé, Acta Mater. **53**, 441 (2005).
[45] H. Mei, C. M. Landis, and R. Huang, Mech. Mater. **43**, 627 (2011).
[46] H. Mei, R. Huang, J. Y. Chung, C. M. Stafford, and H.-H. Yu, Appl. Phys. Lett. **90**, 151902 (2007).
[47] D. Vella, J. Bico, A. Boudaoud, B. Roman, and P. M. Reis, Proc. Natl. Acad. Sci. USA **106**, 10901 (2009).
[48] A. J. Nolte, J. Young Chung, C. S. Davis, and C. M. Stafford, Soft Matter **13**, 7930 (2017).
[49] K. Johnson, K. Kendall, and A. Roberts, Proc. R. Soc. A **324**, 301 (1971).
[50] S. T. Milner, J. F. Joanny, and P. Pincus, Europhys. Lett. **9**, 495 (1989).
[51] Equations (8a) and (9a) each are of second order and thus together require four boundary conditions. In addition, Eqs. (8c), (8d), (9c), and (9d) are each of first order and require another four boundary conditions. Last, the ninth boundary condition is required since the constant ℓ is unknown.
[52] C. Majidi and G. G. Adams, Mech. Res. Commun. **37**, 214 (2010).
[53] O. Oshri and H. Diamant, Phys. Chem. Chem. Phys. **19**, 23817 (2017).
[54] A. Magnusson, M. Ristinmaa, and C. Ljung, Int. J. Solids Struct. **38**, 8441 (2001).
[55] M. Abramowitz and I. A. Stegun, *Handbook of Mathematical Functions*, 9th ed., Dover Books on Mathematics (Dover Publications, Mineola, 1965).
[56] O. Oshri, F. Brau, and H. Diamant, Phys. Rev. E **91**, 052408 (2015).
[57] G. Napoli and S. Turzi, Meccanica **52**, 3481 (2017).
[58] G. Napoli and S. Turzi, Proc. R. Soc. A **471** (2015).
[59] Here, we neglected structural transitions involving folds because the phase diagram will encompass greater complexity. In future studies, however, we will analyze such transitions.
[60] Note that Eqs. (33b) and (34) are independent of K after dimensions are retrieved.
[61] P.-G. de Gennes, B.-W. Francoise, and D. Quere, *Capillarity and Wetting Phenomena* (Springer, Berlin, 2004).
[62] T. J. W. Wagner, *Elastocapillarity: Adhesion and Large Deformations of Thin Sheets*, doctoral thesis, University of Cambridge (2013).
[63] D. A. Dillard, B. Mukherjee, P. Karnal, R. C. Batra, and J. Frechette, Soft Matter **14**, 3669 (2018).
[64] U. Seifert, Phys. Rev. A **43**, 6803 (1991).
[65] M. Deserno, M. M. Müller, and J. Guven, Phys. Rev. E **76**, 011605 (2007).
[66] C. Majidi and K. tak Wan, J. Appl. Mech. **77**, 041013 (2010).
[67] X.-H. Zhou, J.-L. Liu, and S.-L. Zhang, Colloids Surf. B **110**, 372 (2013).